Structural Analysis and Electronic Properties of Negatively Charged TCNQ: 2D Networks of $(TCNQ)_2Mn$ Assembled on Cu(100)†

X. Q. Shi,‡ Chensheng Lin,‡,¶ C. Minot,‡,§ Tzu-Chun Tseng,|| Steven L. Tait,*,||,⊥ Nian Lin,||,# R. Q. Zhang,‡ Klaus Kern,||,▽ J. I. Cerdá,○ and M. A. Van Hove*,‡

Department of Physics and Materials Science, City University of Hong Kong, Hong Kong, China, Laboratoire de Chimie Théorique, Université Pierre & Marie Curie, Paris 6, CNRS, UMR7616, Case 137, 4 place Jussieu, Paris, F-75252 Cedex France, Max Planck Institute for Solid State Research, Heisenbergstrasse 1, D-70569 Stuttgart, Germany, Department of Chemistry, Indiana University, Bloomington, Indiana 47405, Department of Physics, The Hong Kong University of Science and Technology, Clear Water Bay, Hong Kong, China, École Polytechnique Fédérale de Lausanne, 1015 Lausanne, Switzerland, and Instituto de Ciencia de Materiales de Madrid, ICMM-CSIC, Cantoblanco, 28049 Madrid, Spain

Received: May 4, 2010; Revised Manuscript Received: July 20, 2010

A compound two-dimensional monolayer mixing Mn atoms and 7,7,8,8-tetracyanoquinodimethane (TCNQ) molecules was synthesized by supramolecular assembly on a Cu(100) surface under ultrahigh-vacuum conditions. The interactions in the $Mn(TCNQ)_2$ network and in the full system are analyzed from a molecular orbital perspective and in the light of scanning tunneling microscopy (STM) imaging and simulations. Structural, electronic, and magnetic properties are studied in detail using density functional theory (DFT) calculations. In the absence of Cu and depending on the theoretical method used, the TCNQ species can be formally described as either dianions $TCNQ^{2-}$ interacting with Mn^{4+} cations according to ligand field theory (using GGA calculations) or, alternatively, as radical monoanions interacting with Mn^{2+} cations in a high spin state (using GGA+U calculations). In the complete system including a Cu substrate, whatever theoretical method is used, TCNQs appear as dianions interacting with both Mn^{2+} cations in a high spin state (d^5) and charged copper surface atoms.

1. Introduction

Much interest has focused these last decades on organic charge-transfer (CT) salts that display unusual solid state properties such as metallic conductivity, superconductivity, magnetic, and optical properties. The motivation behind research on these materials is twofold: (i) there is a wealth of fundamental solid-state chemistry and physics to be uncovered, and (ii) there are potentially many far-reaching technological applications within the arena of molecular electronic devices.[1]

During the past decades, many salts of TCNQ (7,7,8,8-tetracyanoquinodimethane) were studied.[2−5] TCNQ is indeed the most famous organic π-acceptor component for these CT salts, and the population of its lower molecular orbital controls its main electronic properties. This population can be 2e in the dianion $TCNQ^{2-}$ or 1e in a radical monoanion, or less than 1e in the presence of metal atoms. This depends on the stoichiometry and on the coordination (the terms dianion and monoanion are used here in their usual formal sense, with integer oxidation numbers; the "actual" atomic charges depend on how charge is partitioned between ions and can be nonintegers). The radical monoanion structures for TCNE (tetracyanoethylene) and TCNQ are well characterized.[6] The radical may be stabilized by dimerization[7,8] or by interaction with donors when forming salts.[9] TCNE and TCNQ acceptor dianions have also been stabilized.[6] The TCNQ dianion can combine with metal complexes, thus forming adducts.[10−14] The existence of the TCNQ dianion in a vacuum on the microsecond time scale was demonstrated in electron transfer from sodium vapor to monoanions of high translational energy.[15] The charge transfer to the dianion allows oxidizing metal atoms to generate metal cations in a high spin state, thus causing a large magnetization.

TCNQ was chosen to coordinate with transition metal ions for preparing molecular magnets because large local superexchange interactions are expected between the high spin state of the metal ions and organic spin carriers. Recently, we presented the assembly of a two-dimensional $Mn(TCNQ)_2$ coordination network on a Cu(100) surface and characterized the network by combined STM, LEED, and DFT studies, emphasizing the interpretation of the experiments.[16] We concluded that a high magnetization occurs due to the presence of Mn^{2+} ions in a high spin state. The current paper gives a more complete and detailed theoretical analysis of the various interactions in this particularly interesting system, based on DFT and DFT+U calculations and a more sophisticated approach to modeling STM.

2. Calculation Details

In our DFT calculations, the structures were optimized with the VASP package,[17−19] which uses a periodic approach with plane waves as the basis set (the resulting atomic coordinates are provided in the Supporting Information of this Article). The

* To whom correspondence should be addressed. Email: vanhove@cityu.edu.hk.
† Part of the "D. Wayne Goodman Festschrift".
‡ City University of Hong Kong.
§ Université Pierre & Marie Curie.
|| Max Planck Institute for Solid State Research.
⊥ Indiana University.
The Hong Kong University of Science and Technology.
▽ École Polytechnique Fédérale de Lausanne.
○ ICMM-CSIC.
¶ Current address: Fujian Institute of Research on the Structure of Matter, Chinese Academy of Sciences, Fuzhou, China.

10.1021/jp104954w
Published on Web 08/04/2010

projected augmented wave method[20,21] was adopted. The exchange correlation functional was treated within the generalized gradient approximation (GGA) of Perdew and Wang[22,23] with the Vosko−Wilk−Nusair (VWN) interpolation of the correlation energy.[24] The kinetic energy cutoff was set to 400 eV. Five-layer metal slabs, with 10 Å of vacuum between slabs, were used to simulate the surface.

The top three copper layers and all of the adsorbate atoms were allowed to relax until the largest force component was smaller than 0.04 eV/Å, while the bottom two copper layers were fixed to the experimental bulk Cu geometry. Integrations in the first Brillouin zone were performed using a Monkhorst−Pack grid of (2 × 2 × 1) *k*-points. The details of the supercell employed will be given in the next section.

Since electronic correlations for the tightly bound localized states of the transition metals are often poorly described by standard LDA/GGA functionals, it is common practice to include Hubbard-type terms as in the so-called U approach. Therefore, we performed calculations for both the GGA and GGA+U formalisms.[25−27] For the latter, we follow the work of Dudarev et al.[27] and use a single effective parameter, $U_{\mathrm{eff}} = U - J$, for the Mn atoms. As a rough estimation, we set U_{eff} for Mn to 4.2 eV.[28]

The molecular calculations were performed using Gaussian 03 code.[29] The hybrid density functional B3LYP (Becke, three-parameter, Lee−Yang−Parr) for the exchange-correlation potential[30] and the split-valence basis set 6-311++G(2df,2p) were adopted.

3. Experiment

Experimental work on self-assembled $Mn(TCNQ)_2$ networks on Cu(100) has been described in detail in a recent publication[16] and is summarized briefly here. The experiments were conducted under ultrahigh vacuum conditions ($<3 \times 10^{-10}$ mbar) using single crystal Cu(100) samples, which were cleaned by cycles of sputtering and annealing. First TCNQ molecules and then Mn atoms were vapor deposited to the sample using Knudsen cell and electron beam evaporators, respectively. The sample was held at 160 K during the deposition steps and then annealed for 15 min at about 400 K before in situ characterization by STM, X-ray photoelectron spectroscopy, and low-energy electron diffraction.

STM imaging found a highly ordered network with $Mn(TCNQ)_2$ composition, shown and interpreted in Figure 1. The network lattice structure is described in detail below. Two symmetry-equivalent orientational domains of the lattice are observed on the surface which are distinguished by unit cell orientations of ±8.1° from the [010] direction and opposite organizational chirality in the ordering of the TCNQ molecules around the Mn center (one orientational domain is shown in Figure 1). The structures were imaged and found to be very stable at room temperature.

4. Description of the Structure of $Mn(TCNQ)_2$ Adsorbed on Cu(100)

The (5 × 5)R36.9° superlattice formed by the Cu atoms and the adsorbates is square (cf. the red unit cell in Figure 2); its unit cell contains two TCNQ molecules and a Mn atom in the overlayer, and 25 Cu atoms per substrate layer. The experimental image allows two slightly different and thus inequivalent models for this system, beyond the equivalent models obtained by simple rotational and mirror symmetry operations: we call them the "aligned model" and "twisted model". They are physically difficult to distinguish, whether in terms of STM imaging, total energy, bond lengths, electronic structure, or magnetic properties. The "aligned model" is shown in Figure 2 and discussed in the following, while the "twisted model" will be addressed in section 9.

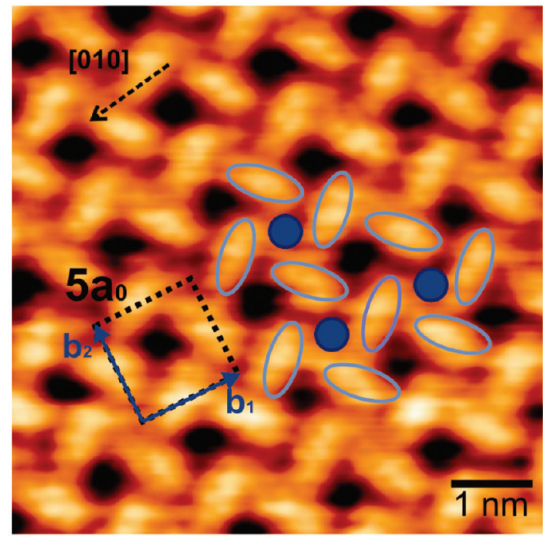

Figure 1. High-resolution STM topograph of the $Mn(TCNQ)_2$ network, showing the [010] direction within the Cu(100) substrate surface, the (5 × 5)R36.9° unit cell of the self-assembled superstructure, and approximate outlines of Mn atoms (circles) and TCNQ molecules (ellipses). STM image recorded with −0.72 V sample bias and 0.26 nA tunneling current.

There are C_4 symmetry axes at the centers of two different (yellow) squares formed by the four nitrogen atoms of adjacent TCNQ molecules. A Mn atom occupies the center of the smaller of these squares, while each of the other four N atoms forming the larger square is almost directly above a (second-neighboring) Cu atom. The smaller square has roughly the dimension of the primitive (1 × 1) unit cell of the Cu lattice and is slightly rotated relative to it. The other square, somewhat larger, almost matches the $(\sqrt{2} \times \sqrt{2})R45° = c(2 \times 2)$ cell of the Cu(100) lattice. The adjacent N atoms in these squares belong to different TCNQ molecules; along an edge of a square, they belong to TCNQ molecules that have different orientations, while the diagonals of the square connect TCNQ molecules with the same orientation due to translation symmetry. The lattice vectors in terms of the 2D Cu(100) lattice vectors (a_x, a_y) are ($4a_x + 3a_y$) and ($-3a_x + a_y$), giving the superlattice matrix notation

$$\begin{pmatrix} 4 & 3 \\ -3 & 4 \end{pmatrix}$$

equivalent to the Wood notation (5 × 5)R36.9°, which reflects that the superlattice unit cell is rotated relative to the (1 × 1) cell of the Cu lattice (the integer dimensions 5 result from $5^2 = 4^2 + 3^2$). The cell parameter is therefore $5d = 12.78$ Å, with $d = 2.556$ Å being the bulk Cu−Cu nearest neighbor distance ($\sqrt{2}d = a = 3.615$ Å = Cu fcc unit cell parameter).

5. Geometry of the Neutral and Charged TCNQ Molecule

The geometry of TCNQ in the gas phase shows alternating bonds in agreement with the localization of the double bonds on C_1-C_2 and C_3-C_3 as labeled in the Lewis structure for the neutral molecule shown in the inset of Table 1. This mainly originates from the phase relationship of the HOMO of the

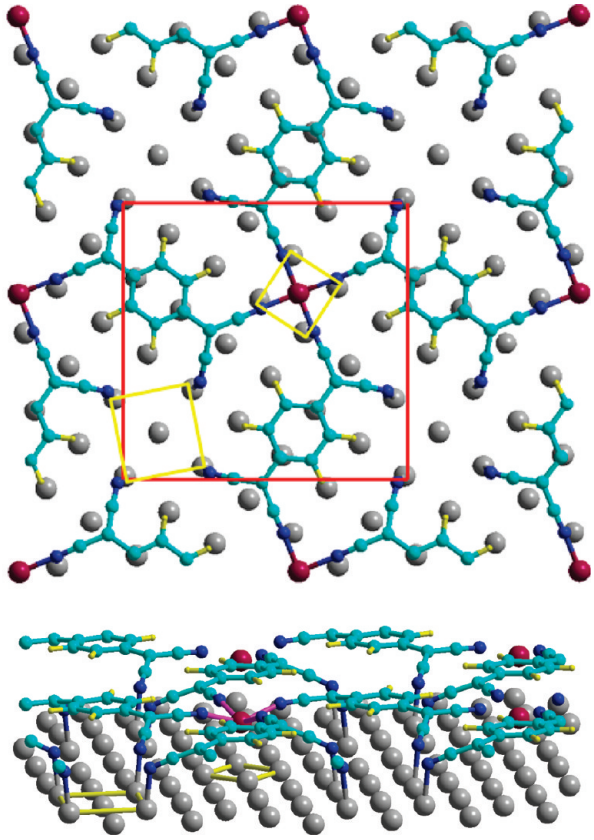

Figure 2. (a) Top view and (b) oblique view of the "aligned model" of the adsorbed system Cu(100)-(5 × 5)R36.9°-Mn+$(TCNQ)_2$. "Aligned" refers to the orientation of the long TCNQ axis being essentially parallel to rows of Cu atoms, unlike in the slightly different "twisted model" described in section 9. The system's unit cell is drawn as a red square. The Cu, Mn, C, N, and H atoms are shown as gray, purple, light blue, dark blue, and yellow balls, respectively. A primitive (1 × 1) cell and a ($\sqrt{2}$ × $\sqrt{2}$)R45° = c(2 × 2) supercell of the Cu(100) surface are also shown as yellow squares in the top and side views; they roughly correspond to two squares formed by four N atoms. Only the outermost layer of Cu atoms is shown here for clarity, but a total of five layers were used in the calculation.

molecule (of B3U symmetry,[31] as shown in Figure 4). We can view it as the out-of-phase combination of all the bonding π orbitals localized on each double bond.

In the presence of an electron donor (an Mn atom or the Cu surface), we expect TCNQ to become negatively charged, filling the LUMO of B2G symmetry; cf. Figure 4. This orbital may be seen as the in-phase combination of all the antibonding π^* orbitals localized on each double bond. The filling of this orbital reverses the bond length alternation observed in the ground state: every double bond is weakened, with elongated distances due to the filling of the π^* orbitals; the σ bonds connecting them acquire a partial π bonding character due to the in-phase combination. This can be seen in Table 1 for the monoanion radical and to a greater extent for the dianion, for the network and for the protonated $TCNQH_4^{2+}$, the latter being a simple local model of the TCNQ network. The optimized distances for these structures exhibit shortened C_0-C_1 distances, elongated C_1-C_2 distances, and nearly equivalent distances within the ring. When the B2G orbital is completely filled, the dianion may be represented by the Lewis formulas displayed in Figure 3. The weakening of the C_1-C_2 double bond to a single bond in the dianion state allows greater flexibility in bending this bond, which has been cited as a critical step for TCNQ bonding and the resulting self-assembled island formation on Cu(100).[32]

TABLE 1: Bond Distances in Å in Neutral and Charged Systems, Calculated by VASP and Gaussian as Indicated, with Sketch of the Lewis Structure of Free TCNQ Showing Atom Labeling (N_{Cu} Refers to N Atoms That Bond to Cu in the Full System)[a]

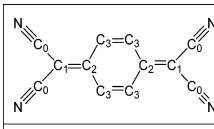	C_0N_{Cu}	C_0-C_1	C_1-C_2	C_2-C_3	C_3-C_3
TCNQ (Gaussian 03) (values in parentheses from ref. 9)	1.153	1.422	1.382 (1.37)	1.443 (1.45)	1.349 (1.35)
TCNQ (VASP)	1.17	1.42	1.40	1.44	1.36
monoanion radical (Gaussian 03)	1.159	1.410	1.426	1.421	1.369
$Mn[TCNQ]_2$ (VASP)	1.18	1.39	1.44	1.42	1.38
dianion $TCNQ^{2-}$ (Gaussian 03)	1.181	1.399	1.475	1.414	1.393
$Mn[TCNQ]_2$/Cu(100) (VASP)	1.18	1.38	1.47	1.39	1.41
$TCNQH_4^{2+}$ (Gaussian 03)	1.153	1.373	1.491	1.396	1.385

[a] Values in parentheses are from ref 9. The different VASP calculations for $Mn[TCNQ]_2$ (for the high- or low-spin state of Mn, with GGA or GGA+U, with or without cell parameter optimization) give negligible variations of the bond lengths. $TCNQH_4^{2+}$ is the protonated form of the dianion shown in Figure 3c.

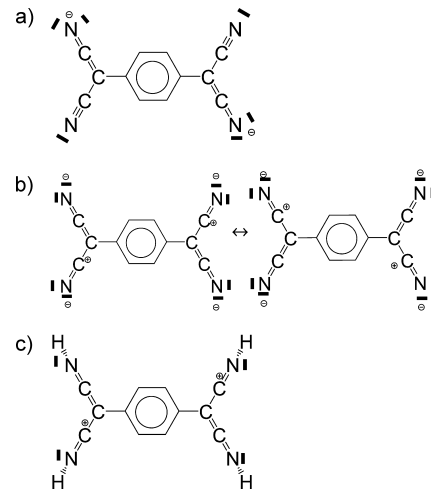

Figure 3. Representations of the TCNQ dianion: (a) allene-like C_1-C_0-N units and cyano structures (C_0N pairs) (resonance makes these functions exchangeable); (b) a more symmetrical representation showing resonance between two positive $C_0-C_1-C_0$ units (allyle-like); (c) $TCNQH_4^{2+}$, also resembling TCNQ after adsorption. The orientation of the π orbitals in the C═N bonds is perpendicular to that of the π orbitals of the $C_0-C_1-C_0$ units and the phenyl rings (the N lone pairs are marked by heavy bars without indication of directionality), making the H atoms in structure c move out of the molecular plane.

We can analyze the geometrical variations by considering three parts of the molecule. Let us refer to the representations shown in Figure 3. The central unit is a nearly 6-fold symmetric ring that resembles an aromatic ring, at variance with the neutral TCNQ whose ring is asymmetric. Second, the $C_0-C_1-C_0$ units remain coplanar with the central ring (before charge transfer) in order to allow conjugation. Two π electrons occupy the lowest π orbital of each $C_0-C_1-C_0$ unit that is isolobal to the allyl cation. The third part is composed of the CN groups whose π orbitals must have an orientation perpendicular to that of the remaining π system ($C_0-C_1-C_0$ units and central hexagonal ring), so the CN π orbitals must be oriented within the TCNQ plane, since the C_0 carbons have sp hybridization, as found in the allene structure. This in turn makes the electron pairs of the

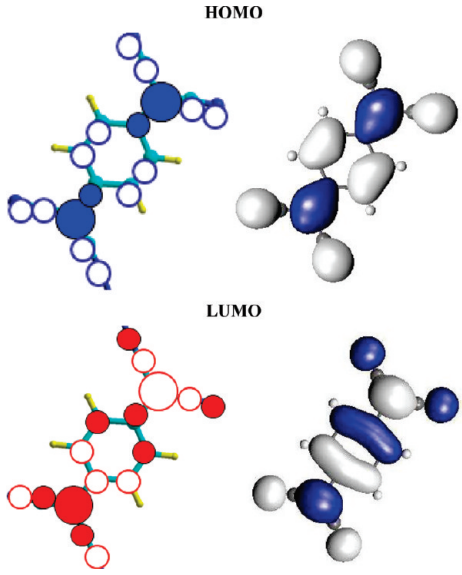

Figure 4. Frontier orbitals of the TCNQ molecule. The HOMO (of B3U symmetry) is the out-of-phase combination of all the bonding π orbitals localized on the bonds as appearing in the Lewis formula (C_0N, $C_1{=}C_2$, $C_3{=}C_3$, cf. Table 1). The LUMO (of B2G symmetry) is the in-phase combination of all the antibonding π orbitals localized on each double bond. This in-phase character appears between C_0 and C_1, C_2, and C_3, whereas nodes are present on the double bonds from the Lewis formula.

N atoms point out of the TCNQ plane on both sides and orients half of them such that they interact strongly with the underlying Cu atoms.

Figure 3 shows several representations of the dianion with indication of the formal charges; structure a contains two allene-like structures and two cyano structures. Structure b is more symmetrical and shows four nitrogen atoms with negative charges. Four N lone pairs were already present in the neutral TCNQ, so there is a total of eight lone pairs in the dianion (two per N atom). The four other pairs arise from the six remaining electrons of the π conjugated system of the TCNQ (16 electrons minus the 10 that are still filling the conjugated π system) and from the two lone pairs of the dianion charge. In structure c, we have added four protons that take the place of the four Cu atoms and the Mn, making this model system isolobal to the adsorbed TCNQ.

6. Interaction between the Four N Atoms with Four Nearby Cu Atoms or Mn

A set of four N atoms forming any small square in Figure 2 interacts through their N σ lone pairs and through the molecular π system. The interaction involving the four σ lone pairs is that of four independent atomic orbitals and is not *k*-dependent. By contrast, the delocalization of the π orbitals makes their phase relationship on the four interacting N atoms dependent on the orbital symmetry and on the *k*-point. In this case only, we expect band dispersion for the orbitals.

The set of four Cu atoms that are close to the four N atoms forms a square (cf. the midsize square drawn in Figure 2a) and is characterized by four valence orbitals (4s) that can combine with A1, A2, and E symmetry (see Figure 5). Similarly, the four nearby N σ lone pairs pointing toward the Cu atoms also generate four MO orbitals of the same local symmetry. There is always a good match between these orbitals which does not depend on the *k*-point, and therefore, we do not expect band dispersion for the orbitals associated with this interaction.

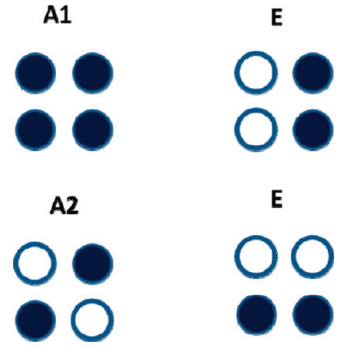

Figure 5. Local symmetries for four Cu atoms. For the TCNQ orbitals labeled in the text as B3U, the patterns A1 and A2 are found at the Γ point of the band structure and pattern E at point M. This is reversed for TCNQ orbitals labeled as B2G. At Γ, the orbitals along a diagonal are in phase, whereas, at M, they are out of phase.

When Mn is in the TCNQ plane, there is one strong σ interaction of A2 symmetry involving a d orbital ($d_{x^2-y^2}$, calling *x*,*y* the directions to the N atoms) of Mn and the $2sp_\sigma$ orbital of the N (pointing in the direction opposite to C). This interaction is always present. To understand the electronic properties, we are, however, more interested in the d orbitals close to the Fermi level (E_F) that are π orbitals (d_{xz} and d_{yz}) and can interact with the p_z orbitals of the N atoms; these orbitals have local E symmetry and interact only when their phases match the phase relationship of the p_z(N) orbitals. Periodicity introduces then a constraint between the phase relationships of the p_z(N) orbitals on a diagonal of the square filled by the Mn atom: the N atoms belong to TCNQs that are related by translation symmetry; this imposes different relationships depending on the *k*-point and the symmetry of the MO. At Γ, the p_z(N) orbitals along a diagonal are in phase for the B3U MO (D_{2h} group). The periodicity and the MO symmetry preserve the phase, thus forming locally A1 and A2 patterns; cf. Figure 5. This is reversed for the B2G orbital, since the MO symmetry changes the phase. Therefore, interaction at Γ with Mn E orbitals is then only possible for B2G. At M, the relations are reversed, since periodicity reverses the phases: in phase for the B2G (noninteracting) and out of phase for B3U (interacting).

7. Electronic Description

In the following, we analyze stepwise the formation of the complete adsorption system. Without Mn and Cu, the layer of TCNQ gives sharp peaks in the density of states (DOS) associated with the molecular orbitals of the TCNQ. Each level is degenerate, since there are two TCNQs per unit cell. The interaction between the molecules is negligible due to the large spacing between them, imposed by the positions given by the not-yet-present Cu substrate.

7.1. Electronic Description of the $Mn(TCNQ)_2$ Layer Using GGA. When Mn is the only interacting metal (TCNQ with Mn but without Cu), the interstitial space filled by the Mn is small and the system remains planar with D_{4h} symmetry. The small size of the filled square results from adaptation to the unique interaction with Mn instead of sharing of electrons with the Cu atoms. The Mn−N distance is 1.876 Å, which is quite short compared to the sum of covalent radii (2.10 and 2.32 Å for the low- and high-spin states of Mn, respectively) or ionic radii (2.12 and 2.26 Å, respectively). Note, however, that these small distances do not mean that the unit cell is compressed by the substrate (the substrate is now absent, but its lattice constant here fixes the unit cell dimension); without Mn as "glue", the

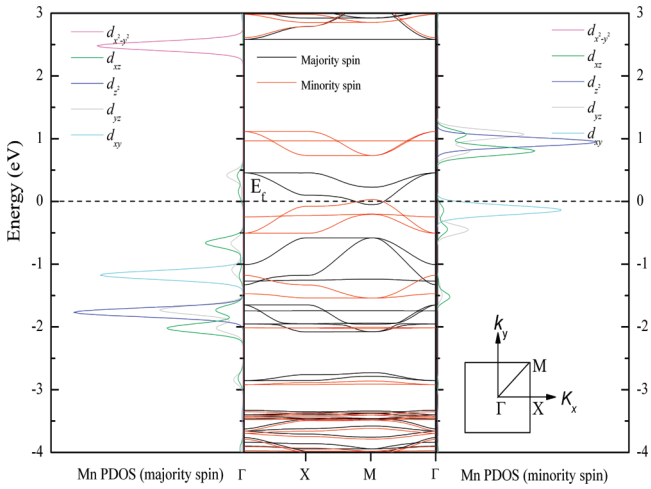

Figure 6. Bands and DOS projected on the Mn-d states for $(TCNQ)_2Mn$ (low spin state, no Cu present). Note that the *x* and *y* labels of the d orbitals are defined for the ligand field and rotated relative to the cell vectors; i.e., the *x* and *y* directions are defined along Cu−Mn vectors.

four N of the unfilled square would repel each other and the optimized lattice constant (without Cu) would be slightly larger than in the presence of the Cu substrate (13.15 Å vs 12.78 Å).

From GGA, the magnetization for the ground state is 1 μ_B. A high spin (HS) state with a magnetization of 3 μ_B lies 0.296 eV above this low spin (LS) state. The Mn donates four electrons and formally becomes Mn^{4+} with a low spin configuration $d_{xy}^2 d_{z^2}^2$, while the TCNQ molecules become dianions. The total spin, 1 μ_B, is entirely localized on the Mn ion and arises from the large spin split of the noninteracting d_{z^2} states. The populations of the d orbitals of Mn are those predicted from ligand field theory. The d_{xy} orbital is occupied, and the d_{xz}, d_{yz}, and $d_{x^2-y^2}$ orbitals are empty.

The frontier orbitals are π orbitals localized on the TCNQ dianion with some d_{xz} and d_{yz} contributions. Neglecting a very small overlap at M (see Figure 6), the bands originating from them are filled or empty, in agreement with a dianion structure for TCNQ and excluding that of a monoanion radical. The HOMO of the TCNQ molecule is of B3U symmetry. The LUMO (B2G) is of particular interest due to the electron transfer to the TCNQ, since it is populated for the dianion and becomes then the HOMO. Since there are two TCNQs per unit cell, we have two degenerate bands below E_F that originate from this MO. The TCNQ system may be viewed as two chains propagating in the two perpendicular directions of the lattice, labeled $x+y$ and $x-y$ to orient the axes toward the ligands. The π orbitals interact with the d_{xz} and d_{yz} orbitals of Mn. The bonding combinations are below E_F and are mostly localized on the TCNQ orbitals; the antibonding combination is above E_F, mostly localized on the Mn^{4+} ion.

There is band dispersion since the B2G orbital interacts at **Γ** (lower in energy) while it does not at **M** (higher in energy); see Figure 6. In Figure 6, we also see these two bands below E_F duplicated for majority spin (black) and minority spin (red). At **X**(π,0), degeneracy is lifted, because the band which maintains the phase is interacting while the band which changes phase is not interacting. This leads to a "hysteresis shape" along the **Γ−X−M** direction. At the special *k*-point **X**(π,0), the bands obtained by permuting the *x* and *y* axes would give the same pattern. Above E_F, we have the antibonding combinations of these orbitals, which are more localized on the d_{xz} and d_{yz} orbitals of Mn; they have the opposite dispersion. In Figure 6, two flat bands of minority spin localized on the Mn ion are superposed on these π orbitals at the Fermi level: the d_{xy} spin orbital (occupied) and the d_{z^2} spin orbital (unoccupied).

7.2. Electronic Description of the $Mn(TCNQ)_2$ Layer Using GGA+U. The GGA+U method forces the Mn into a HS (high spin) state which is more stable than the LS (low spin) state by 0.675 eV. The Mn−N distance is increased from 1.94 to 2.09 Å (for the Mn LS and HS states, respectively), revealing weaker Mn−N interactions. Mn may be viewed as Mn^{2+} with five unpaired d electrons leading to an atomic magnetic moment of 5 μ_B. Each TCNQ molecule is a radical anion with a spin of −1 μ_B, providing a total magnetization for the system of +3

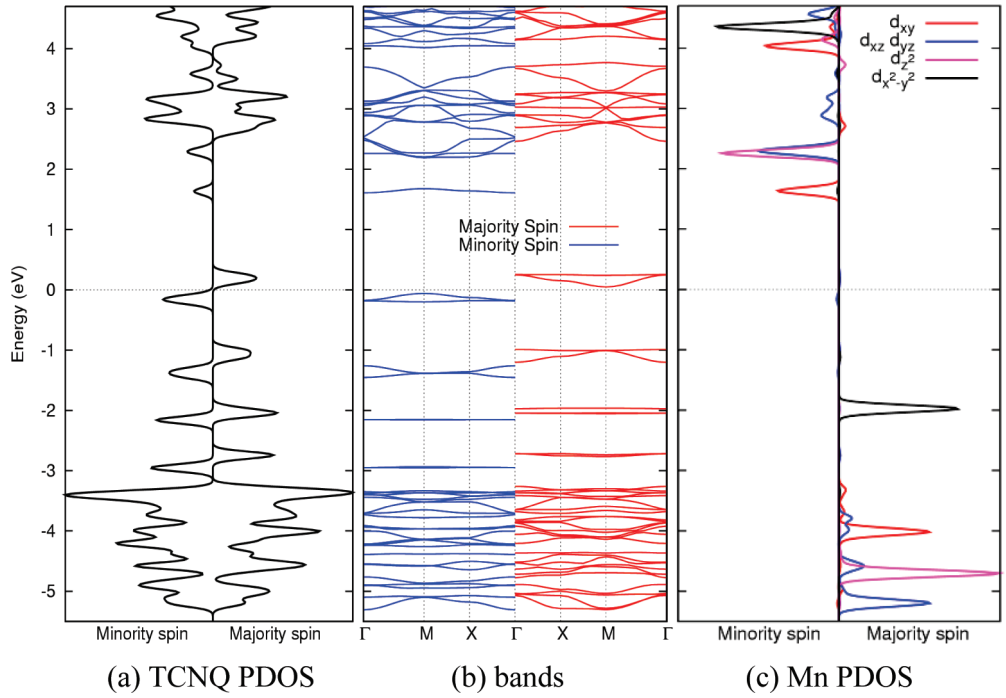

Figure 7. Bands and PDOS for $(TCNQ)_2Mn$ with Hubbard U (high spin state, no Cu present).

μ_B. The spin in the TCNQ is delocalized, since it arises solely from the B2G orbital split. The dominant contributions are on the four C_1 atoms (−0.35 |e|), the eight N (−0.45 |e|), and the four C_2 (−0.17 |e|). The ferromagnetic arrangement between the Mn atom and the TCNQ radicals of majority spin (magnetization of +7 μ_B) is 0.12 eV higher in energy than the antiferromagnetic arrangement of the Mn and TCNQ radicals (magnetization of +3 μ_B). On the other hand, the ferromagnetic arrangement of the Mn centers is 0.19 eV lower in energy than their antiferromagnetic arrangement (for the doubled $c(2 \times 2)$ supercell built from two (5×5)R36.9° unit cells).

The band dispersion is strongly modified by the addition of a Hubbard U (cf. section 2), as shown in Figure 7. The d(Mn) levels of the Mn^{2+} ions are shifted away from the Fermi level (below for majority spin, above for minority spin) and only the TCNQ π orbitals remain in the energy range close to the Fermi level that splits the B2G band into a contribution of minority spin (below) and majority spin (above).

7.3. Electronic Description of the Full System Using GGA+U. In the calculation for the full system (adsorption of TCNQ and Mn on five Cu layers), the total spin per unit cell is $\mu = 5\ \mu_B$. The PDOS shown in Figure 8 shows a spin polarization that comes exclusively from the Mn atoms which should be seen as Mn^{2+} ions with one electron on each d atomic level (d^5 in the HS state). The ferromagnetic configuration of the Mn^{2+} ions is more stable than the antiferromagnetic configuration by only 5 meV (per Mn unit).

The Mn−N distances, 2.15 Å, which are larger than those for the low spin state, are consistent with the absence of a strong field effect on the Mn. After optimization, the Mn atom does not remain in the plane of the TCNQ layer but moves toward the Cu substrate; it is thus oriented to interact favorably with the nitrogen electron pairs pointing down to the Cu. The Bader charge analysis[33,34] also confirms the oxidation state +2 for Mn. The calculated value, +1.33 |e|, is large even though smaller than the formal charge due to delocalization. The charges on each TCNQ molecule, −1.38 |e|, and on the copper slab, 1.43 |e|, also reveal the dianion character of the molecules and the charge transfer from the Cu. We conclude from this that the formal electron transfer from Mn to the TCNQs is two electrons per unit cell. The TCNQ and the Cu do not participate in the spin polarization, as confirmed by the PDOS analysis (see Figure 8): spin up and spin down peaks occur at the same energy. The two TCNQs remain symmetry equivalent and, being "closed shell" systems in which all the electrons are paired, should receive a total of two electrons each. The two missing electrons are given by the Cu atoms engaged in Cu−N bonds. The Bader analysis indeed shows a large global charge (+1.43 |e|) on them.

Note that the U correction is localized on Mn, and that for the full system the magnetic moment, the charge transfer, and the Mn−N bond length are not sensitive to the U correction. For example, for $U_{eff} = 4.2$ eV, the magnetic moment for the Mn atom is $\mu = 4.9\ \mu_B$, while, for $U_{eff} = 0$ eV, it becomes $\mu = 4.74\ \mu_B$. The U factor is a correction to the functional for the Mn centers that was used previously to obtain a match between experimental and calculated STM images.[25−27] The only obvious difference due to the U correction is the change of the Mn-d PDOS, as shown in Figure 8a and c. This widened band gap at the Mn atoms is essential for accurate simulation of the STM images, as compared with experimental results. The necessity of the Hubbard U correction may be a general effect for such surface systems of ligand coordinated metal centers, especially for the metals with tightly bound localized d orbitals.

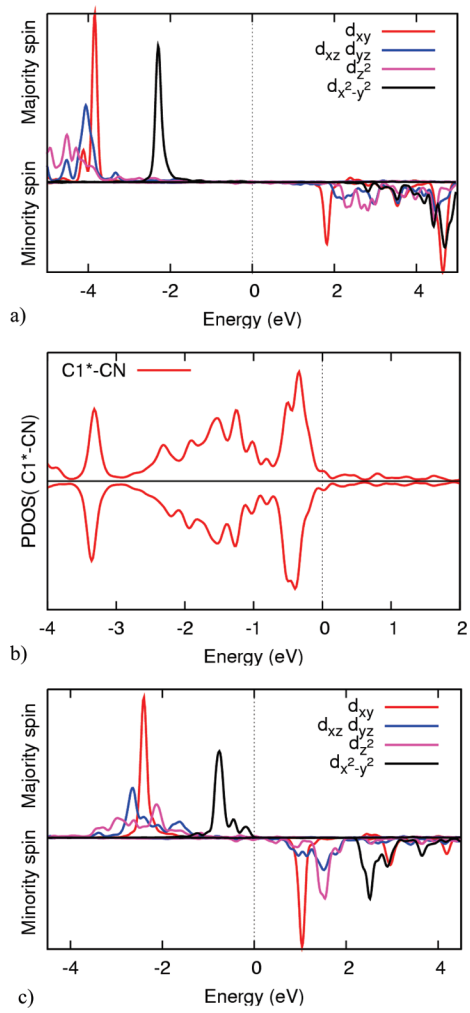

Figure 8. (a) DOS for $Mn(TCNQ)_2/Cu(100)$ projected on the Mn-d states, with U correction. Each of the five d Mn orbitals is occupied by a single electron. (b) PDOS on the TCNQ (projection on C_1 atom). The TCNQ does not contribute to the spin polarization. There are four TCNQ levels in the range from E_F to $E_F - 3.6$ eV, accounting for eight electrons. (c) DOS for $Mn(TCNQ)_2/Cu(100)$ projected on the Mn-d states, without U correction. Each of the five d Mn orbitals is occupied by a single electron.

The addition of four Cu atoms to the $Mn(TCNQ)_2$ layer at the positions of the nearby Cu atoms of the Cu layer makes the structure similar to $TCNQH_4^{2+}$. The four Cu atoms always provide a good match with the N orbitals, so there should not be strong band dispersion. Four N−Cu bonds are formed, two arising from a B3U orbital and two from a B2G orbital, so that, at every k-point, one of them has appropriate symmetry. Since the orbitals of the Cu atoms have different energy levels, the A1 and A2 orbitals are not degenerate. The A2 component is low in energy, since it matches a Cu_4 molecular orbital that has a high energy level; the A1 component is high in energy, since it matches a Cu_4 molecular orbital that has a low energy level. This is seen in Figure 9 and is the reason for the four peaks of Figure 8b.

8. Simulated STM Images

Figure 10 shows simulated topographic STM images for both occupied states and empty states at various bias voltages.[35] In the images for occupied and empty states at low bias (±0.5 V), the TCNQ molecules appear bright, but the empty states image shows the TCNQ orientation more correctly than the occupied

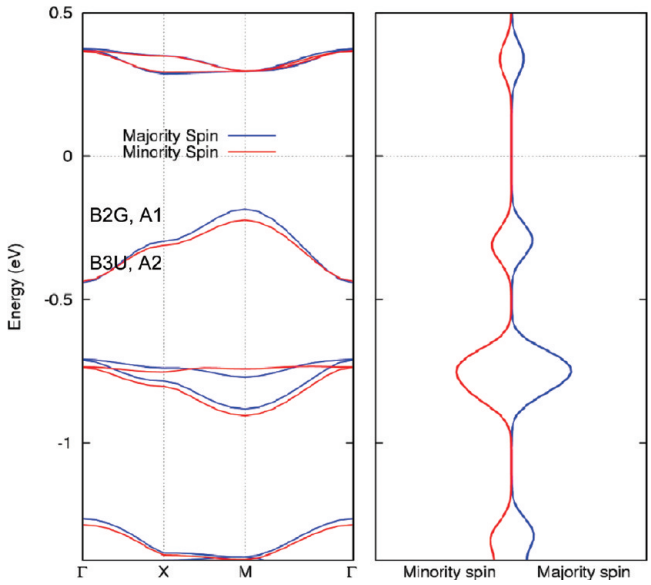

Figure 9. Weak band dispersion of the π orbital levels below E_F (left panel) and projection of the density for atom C_1 (right panel). This is calculated considering only four Cu atoms with $Mn(TCNQ)_2$.

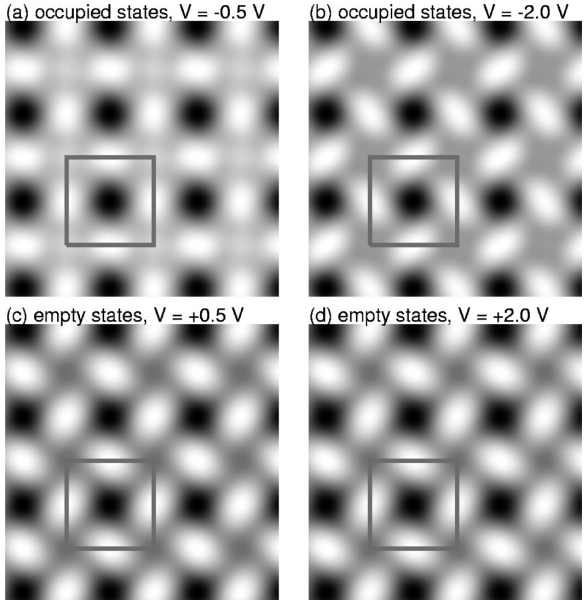

Figure 10. Simulated topographic STM images for both the occupied states (top panels) and the empty states (bottom panels) at various bias voltages V (small in left panels, large in right panels). Mn atoms are located at the four corners of the gray squares; the TCNQ molecules appear bright and the copper layer dark.

states image (Figure 2 shows the TCNQ orientation relative to the Mn−Mn lines of Figure 10). At higher bias (±2.0 V), the empty states image shows the TCNQ orientation clearly, while the occupied states image shows an opposite orientation. This is because the occupied states images at high bias mainly show the phenyl ring of TCNQ, while the phenyl ring has a different orientation relative to the Mn−Mn line.

Some comments are warranted on the methodology of STM image simulation. In the current study, we describe both the sample and the tip in a fully *ab initio* manner, while, in our previous work,[16] we use extended Hückel type (EHT) parameters fitted to *ab initio* electronic structure results. If we can fit the EHT parameters well to the *ab initio* results, we can safely use the EHT description; however, the EHT parameter fitting itself is both time-consuming and far from trivial given the large unit

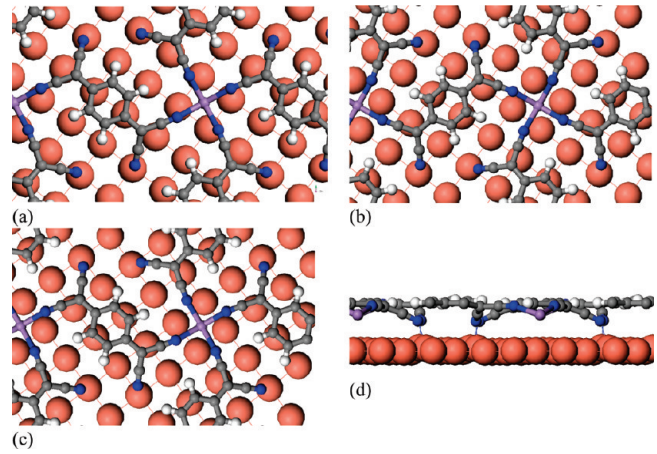

Figure 11. (a) Top view of the "aligned model" (equivalent to Figure 2a). (b and c) Two equivalent representations of the "twisted model". (d) Side view of the "twisted model".

cell size. As a result and on balance, for the system studied here with its complex electronic structure, the full *ab initio* calculation is more efficient, in addition to being more accurate.

9. An Almost-Equivalent Model

As mentioned in section 4, there are two possible inequivalent models for the system under study—the "aligned model" and the "twisted model"—which are difficult to distinguish experimentally.

The twisted model (cf. Figure 11b) can be derived from the aligned model (Figure 11a) as follows: first, note that any TCNQ molecule bonds to two Mn atoms through two N atoms that are diametrically opposed within the molecule; now, leaving the Cu substrate and the Mn atoms fixed, rotate the TCNQ about the surface normal by about 80° so that its two other N atoms bond to Mn atoms (yielding Figure 11b of opposite chirality but very similar local bonding). Another way to achieve this same result is by leaving the overlayer of TCNQs and Mn atoms fixed, mirroring the Cu substrate about a Mn−Mn nearest-neighbor line (yielding Figure 11c, which has the same chirality as Figure 11a and is a mirrored copy of Figure 11b).

The resulting twisted model differs as follows from the aligned model: while in the aligned model the long axis of the TCNQ molecule is lined up with a row of Cu atoms, this TCNQ axis in the twisted model is rotated about 10° from such a row of Cu atoms. This rotation is well within the uncertainty of interpretation of the STM image (Figure 1). The twisted model gives somewhat different C−Cu and H−Cu interactions, which are still very weak, but maintains essentially the same N−Mn and N−Cu bonds, which are still very strong (this can be appreciated in the side view of Figure 11d).

Therefore, the STM imaging, total energy, bond lengths, electronic structure, and magnetic properties all remain very similar from the aligned to twisted model. Specifically, the Cu−N bond is shortened by 0.006 Å, the Mn−N bond is lengthened by 0.007 Å, and the magnetic moment (about 4.9 μ_B in both models) is reduced by 0.03 μ_B. The twisted model is slightly better in energy, by about 0.05 eV per (5 × 5) unit cell, or by about kT per TCNQ at room temperature. Thus, there is a chance that both orientations of TCNQ can coexist at room temperature, but again they may be difficult to distinguish in the STM image or by other means.

Consequently, the complete discussion which we presented for the aligned model in sections 1−8 remains valid to a high degree of accuracy for the twisted model.

10. Conclusions

The following picture of the coadsorbed layer of TCNQ and Mn on Cu(100) emerges.

- Two very similar models can be identified, differing in a ~10° reorientation of the TCNQ molecules that is difficult to distinguish experimentally.
- GGA calculations for the $Mn(TCNQ)_2$ layer favor a low spin state (1 μ_B) with Mn^{4+} interacting with TCNQ dianions, in agreement with ligand field theory.
- GGA+U calculations for the $Mn(TCNQ)_2$ layer give a high spin state (5 μ_B) with Mn^{2+} interacting with TCNQ radical anions with a spin state of 1 μ_B that are opposite to the Mn^{2+} spin. The atomic levels of the Mn atoms are then shifted away from the Fermi level.
- Both GGA and GGA+U calculations for $Mn(TCNQ)_2$/Cu(100) give a high spin state (5 μ_B) with Mn^{2+} interacting with TCNQ dianions. The Cu atoms provide the additional electrons that make the TCNQ into dianions.
- The TCNQ molecules have negative charges that impose a shift in the bond alternation of the double bonds. This shift orients nitrogen lone pairs toward the surface Cu atoms.
- The magnetization is 5 μ_B for $Mn(TCNQ)_2$/Cu(100); it is entirely localized on the Mn^{2+} ions with possibly a ferromagnetic configuration (which is better by only 5 meV compared with an antiferromagnetic arrangement).
- Compared with Mn-free adsorption of TCNQ on Cu(100), we find that the Mn atoms cause the TCNQ molecules to crowd more tightly on the surface: without Mn, each TCNQ occupies 14 (1 × 1) unit cells of the Cu(100), while, with Mn, it occupies only 25/2 = 12.5 such unit cells. The Mn "glue" draws the molecules closer together.

Acknowledgment. This work was supported in part by Hong Kong RGC Grant No. CityU 102408 and by the CityU Centre for Applied Computing and Interactive Media. All of the experimental work was performed at MPI Stuttgart and was supported by the European Science Foundation (ESF) EUROCORES-SONS2 program FunSMARTs II. J.I.C. acknowledges financial support from the Spanish MICINN under Contract No. MAT2007-66719-C03-02. C.M. is grateful to the French Consulate General in Hong Kong and Macau for financial support.

Supporting Information Available: The optimized atomic coordinates for the "aligned" and "twisted" models of $Mn(TCNQ)_2$ adsorbed on Cu(100) are provided in crystallographic information format (CIF). This material is available free of charge via the Internet at http://pubs.acs.org.

References and Notes

(1) Bryce, M. R. *Chem. Soc. Rev.* **1991**, *20*, 355–390.

(2) Melby, L. R.; Harder, R. J.; Hertler, W. R.; Mahler, W.; Benson, R. E.; Mochel, W. E. *J. Am. Chem. Soc.* **1962**, *84*, 3374.

(3) Wudl, F.; Smith, G. M.; Hufnagel, E. J. *J. Chem. Soc., Chem. Commun.* **1970**, 1453.

(4) Hünig, S.; Kiesslich, G.; Scheutzow, D.; Zahradnik, R.; Carsky, P. *Int. J. Sulfur Chem., Part C* **1971**, 10.

(5) (a) Ferraris, J.; Cowan, D. O.; Walatka, V., Jr.; Perlstein, J. H. *J. Am. Chem. Soc.* **1973**, *95*, 948. (b) Miller, J. S.; Zhang, J. H.; Reiff, W. M.; Dixon, D. A.; Preston, L. D.; Reis, A. H., Jr.; Gerbert, E.; Extine, M.; Troup, J.; Epstein, A. J.; Ward, M. D. *J. Phys. Chem.* **1987**, *91*, 4344. (c) Zhao, H.; Heintz, R. A.; Dunbar, K. R. *J. Am. Chem. Soc.* **1996**, *118*, 12844. (d) Heintz, R. A.; Zhao, H.; Ouyang, X.; Grandinetti, G.; Cowen, J.; Dunbar, K. R. *Inorg. Chem.* **1999**, *38*, 144. (e) Vickers, E. B.; Selby, T. D.; Thorum, M. S.; Taliaferro, M. L.; Miller, J. S. *Inorg. Chem.* **2004**, *43*, 6414.

(6) Dixon, D. A.; Miller, J. S. *J. Am. Chem. Soc.* **1987**, *109*, 3656.

(7) Miller, J. S.; Novoa, J. J. *Acc. Chem. Res.* **2007**, *40*, 189–196.

(8) Huang, J.; Kingsbury, S.; Kertesz, M. *Phys. Chem. Chem. Phys.* **2008**, *10*, 2625–2635.

(9) Ueda, K.; Sugimoto, T.; Endo, S.; Toyota, N.; Kohama, M.; Yamamoto, K.; Suenaga, Y.; Morimoto, H.; Yamaguchi, T.; Munakata, M.; Hosoito, N.; Kanehisa, N.; Shibamoto, Y.; Kai, Y. *Chem. Phys. Lett.* **1996**, *261*, 295–300.

(10) Khatkale, M. S.; Devlin, J. P. *J. Chem. Phys.* **1979**, *70*, 1851–1859.

(11) Hama, Y.; Nobuhara, Y.; Aso, Y.; Otsubo, T.; Ogura, F. *Bull. Chem. Soc. Jpn.* **1988**, *61*, 1683–1686.

(12) Schiavo, S. L.; Tresoldi, G.; Mezzasalma, A. M. *Inorg. Chim. Acta* **1997**, *254*, 251–257.

(13) Ohashi, Y. *Chem. Lett.* **1999**, *11*, 1187.

(14) Shimomura, S.; Matsuda, R.; Tsujino, T.; Kawamura, T.; Kitagawa, S. *J. Am. Chem. Soc.* **2006**, *128*, 16416–16417.

(15) Nielsen, S. B.; Nielsen, M. B. *J. Chem. Phys.* **2003**, *119*, 10069.

(16) Tseng, T.-C.; Lin, C.; Shi, X.; Tait, S. L.; Liu, X.; Starke, U.; Lin, N.; Zhang, R.; Minot, C.; Van Hove, M. A.; Cerdá, J. I.; Kern, K. *Phys. Rev. B* **2009**, *80* (15), 155458.

(17) Kresse, G.; Hafner, J. *Phys. Rev. B* **1993**, *47*, 558.

(18) Kresse, G.; Furthmüller, J. *Comput. Mater. Sci.* **1996**, *6*, 156.

(19) Kresse, G.; Furthmüller, J. *Phys. Rev. B* **1996**, *59*, 11169.

(20) Blöchl, P. E. *Phys. Rev. B* **1994**, *50*, 17953.

(21) Kresse, G.; Joubert, J. *Phys. Rev. B* **1999**, *59*, 1758.

(22) Perdew, J. P.; Chevary, J. A.; Vosko, S. H.; Jackson, K. A.; Pederson, M. R.; Singh, D. J.; Fiolhais, C. *Phys. Rev. B* **1992**, *46*, 6671.

(23) Perdew, J. P.; Wang, Y. *Phys. Rev. B* **1992**, *45*, 13244.

(24) Vosko, S. H.; Wilk, L.; Nusair, M. *Can. J. Phys.* **1980**, *58*, 1200.

(25) Anisimov, V. I.; Zaanen, J.; Andersen, O. K. *Phys. Rev. B* **1991**, *44*, 943.

(26) Liechtenstein, A. I.; Anisimov, V. I.; Zaanen, J. *Phys. Rev. B* **1995**, *52*, R5467.

(27) Dudarev, S. L.; Botton, G. A.; Savrasov, S. Y.; Humphreys, C. J.; Sutton, A. P. *Phys. Rev. B* **1998**, *57*, 1505.

(28) Rohrbach, A.; Hafner, J.; Kresse, G. *J. Phys.: Condens. Matter* **2003**, *15*, 979.

(29) Frisch, M. J.; Trucks, G. W.; Schlegel, H. B.; Scuseria, G. E.; Robb, M. A.; Cheeseman, J. R.; Montgomery, J. A., Jr.; Vreven, T.; Kudin, K. N.; Burant, J. C.; Millam, J. M.; Iyengar, S. S.; Tomasi, J.; Barone, V.; Mennucci, B.; Cossi, M.; Scalmani, G.; Rega, N.; Petersson, G. A.; Nakatsuji, H.; Hada, M.; Ehara, M.; Toyota, K.; Fukuda, R.; Hasegawa, J.; Ishida, M.; Nakajima, T.; Honda, Y.; Kitao, O.; Nakai, H.; Klene, M.; Li, X.; Knox, J. E.; Hratchian, H. P.; Cross, J. B.; Bakken, V.; Adamo, C.; Jaramillo, J.; Gomperts, R.; Stratmann, R. E.; Yazyev, O.; Austin, A. J.; Cammi, R.; Pomelli, C.; Ochterski, J. W.; Ayala, P. Y.; Morokuma, K.; Voth, G. A.; Salvador, P.; Dannenberg, J. J.; Zakrzewski, V. G.; Dapprich, S.; Daniels, A. D.; Strain, M. C.; Farkas, O.; Malick, D. K.; Rabuck, A. D.; Raghavachari, K.; Foresman, J. B.; Ortiz, J. V.; Cui, Q.; Baboul, A. G.; Clifford, S.; Cioslowski, J.; Stefanov, B. B.; Liu, G.; Liashenko, A.; Piskorz, P.; Komaromi, I.; Martin, R. L.; Fox, D. J.; Keith, T.; Al-Laham, M. A.; Peng, C. Y.; Nanayakkara, A.; Challacombe, M.; Gill, P. M. W.; Johnson, B.; Chen, W.; Wong, M. W.; Gonzalez, C.; Pople, J. A. *Gaussian 03*, revision C.02; Gaussian, Inc.: Wallingford, CT, 2003.

(30) Becke, A. D. *J. Chem. Phys.* **1993**, *98*, 5648–5652. Lee, C.; Yang, W.; Parr, R. G. *Phys. Rev. B* **1988**, *37*, 785–789.

(31) Note the permutation of axes. In this text, the *z* axis is perpendicular to the molecular plane (*xy*). Conventionally, for the *D2h* group, *z* is the main axis of the TCNQ molecule and the axis perpendicular to the molecular plane is *x*.

(32) Tseng, T.-C.; Urban, C.; Wang, Y.; Otero, R.; Tait, S. L.; Alcami, M.; Ecija, D.; Trelka, M.; Gallego, J. M.; Lin, N.; Konuma, M.; Starke, U.; Nefedov, A.; Woll, C.; Herranz, M. A.; Martin, F.; Martin, N.; Kern, K.; Miranda, R. Charge-transfer-induced Structural Rearrangements at Both Sides of Organic/Metal Interfaces. *Nat. Chem.* **2010**, *2*, 374.

(33) Bader, R. *Atoms in Molecules: A Quantum Theory*; Oxford: New York, 1990.

(34) Tang, W.; Sanville, E.; Henkelman, G. *J. Phys.: Condens. Matter* **2009**, *21*, 084204.

(35) We simulate STM images by using a new version of the GREEN code (ref 36), which is based on a Green's function representation and uses a fully *ab initio* description of both the sample and the tip (with the tunneling Hamiltonian and overlap matrix elements between the tip and the sample described by the Slater−Koster parameters fitted for the simulated system). In the simulation, a Pt tip with a pyramidal shape with the Pt(100) plane parallel to the surface is adopted.

(36) Cerdá, J.; Van Hove, M. A.; Sautet, P.; Salmeron, M. *Phys. Rev. B* **1997**, *56*, 15885. See also http://www.icmm.csic.es/jcerda/.

JP104954W